Data Repository/Supplementary Materials: Shaping post-orogenic landscapes by climate and chemical weathering, Chadwick et al.

Paleoclimate Approximately 30 Mya, drying of Southern Africa occurred due to enhancement of the circum-Antarctic Polar Current and this pattern has persisted to the present (Chase and Meadows, 2007). In the Pleistocene, moisture and temperature fluctuations in the region have occurred due to changing sea-surface temperatures, the incursion of westerly storms into the continental interior due to expanding Antarctic sea ice, and changes in the extent of the Inter-Tropical convergence zone to the north of our study area (Chase and Meadows, 2007; Gasse et al., 2008). The collective influence of these Quaternary fluctuations on climate in southern Africa in the vicinity of Kruger appears to have influenced effective moisture by 20% or less as evidenced by paleo-environmental reconstructions over the last 200 ky in the Pretoria pan (Partridge et al., 2003). In summary, it appears that our study area has not been subject to profound variations in tectonic or climatic forcing in the last 30 Mya and perhaps longer.

Regolith Properties Along Catenas

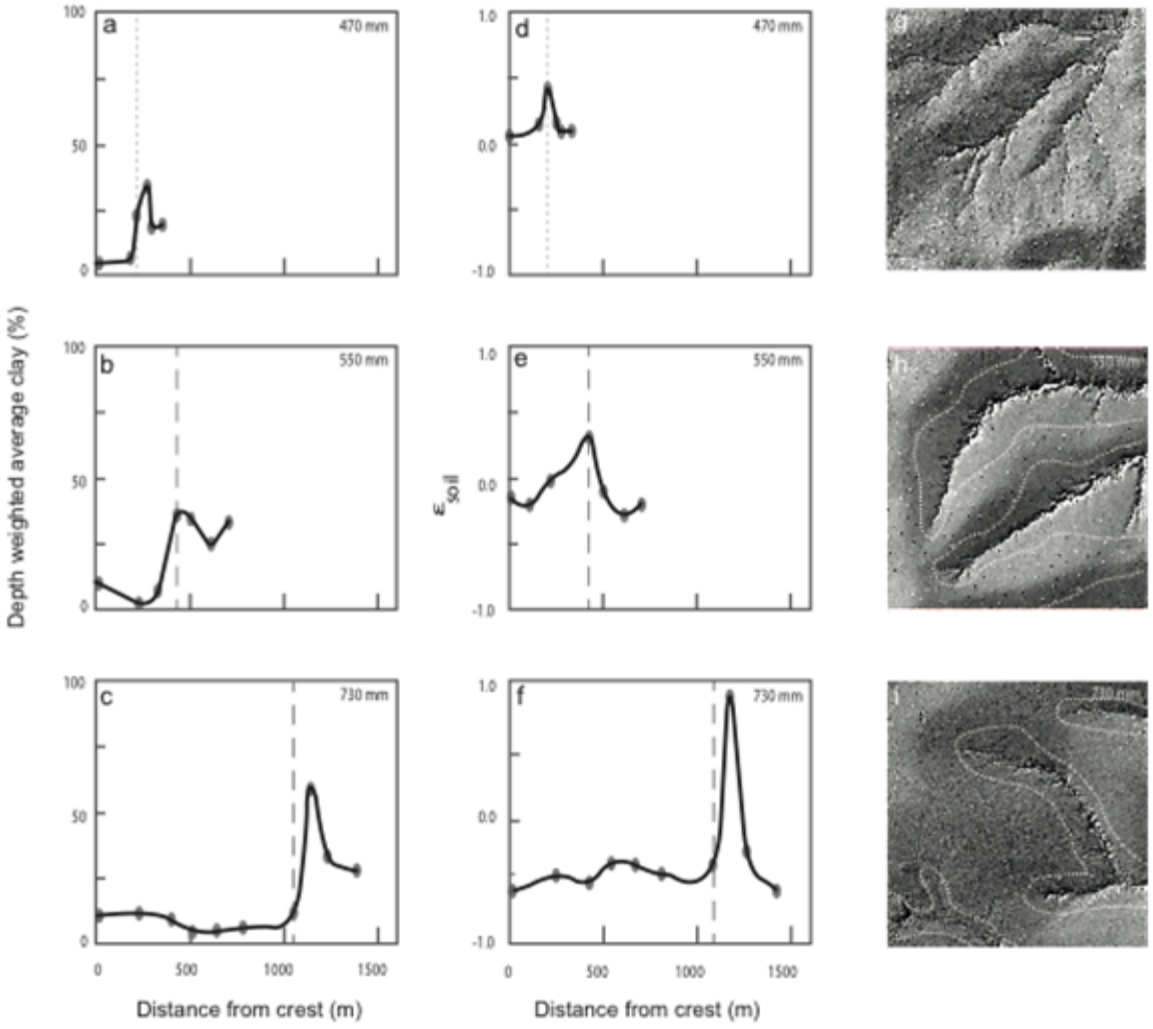

Figure DR1. Clay accumulation in regoliths as a function of distance along catenas (A-C), its impact on profile dilation or collapse (D-F) and the geographic location of seeplines developed at the contact between sandy, highly permeable soils upslope and clay-rich, low permeability soils downslope (dashed lines on G-I). Clay data are depth-weighted average values from surface to hard rock in the dry site and from surface to saprolite contact for the wetter sites and are derived from data presented in Khomo et al., (2011). Soil strain data ($\varepsilon_{i,w} = ((\rho_p C_{i,p})/(\rho_w C_{i,w}))-1$ where ρ is bulk density, C_i is an immobile element concentration (Zr) and the subscripts p and w represent values for rock and regolith, respectively (Brimhall et al., 1992)) are based on density and Zr data from the same soil profiles as those shown in column one (see Khomo et al., 2013). When $\varepsilon_{i,w}$ is <0 collapse is indicated. The seepline (hydrological expression of the sand-to-clay transition) shown as vertical dashed lines in A-F are based on field observations of soil wetness and redoxymorphic features whereas the landscape distribution of seeplines in G-I is shown as dashed lines and determined by a spatial analysis of vegetation and termite mound distributions that are sensitive to clay concentration and water saturation

presented in Levick et al. (2010). Clay accumulation is mediated by through-regolith water flux and hence by effective moisture. In the arid zone, clay redistribution is negligible because overland flow and high evapotranspiration greatly reduces throughflow in soils (Khomo et al., 2011; Bern et al., 2011). As a consequence evidence for a seepline at the sand-to-clay contact exists within soil as redoxymorphic features but cannot be determined as a specific landscape feature (seepline shown as dotted line on A and D, but no seepline shown on G). In the arid catenas dilation of the catena profiles is likely driven by dust inputs whereas in the wetter sites weathering dominates generating collapse at the crests and dilation in parts of the clay-rich zone (Khomo et al., 2013).

Catchment Average Erosion Rates

We measured ^{10}Be concentrations in quartz-rich sediments in 1st through 4th order watersheds (as defined by Strahler, 1957) ranging in size from <1 to >750 km^2 (Table DR1) to determine catchment-averaged erosion rates (Brown et al., 1995; Granger et al., 1996; Bierman and Steig, 1996). This method has been successfully applied in numerous studies of upland landscapes (e.g., von Blanckenburg, 2005 and references within). For each catchment, we separated quartz using standard techniques (Kohl and Nishiizumi, 1992) while PrimeLab (Purdue University) performed the ^{10}Be isolation and measurement. We calculated ^{10}Be production rates for each catchment, correcting for elevation and latitude (Dunai, 2000). Topographic shielding and muogenic production were not accounted for, and contribute to an estimated 5% uncertainty in production rates that is added to the 1σ analytical error. Although we did not quantify the impact of catchment weathering status and quartz content on catchment-averaged erosion rates, we do not expect significant variation as all of the basins sample quartz-rich granitic rocks and the regolith does not have thick saprolite layers, which might skew average catchment erosion rates significantly (Riebe and Granger, 2013).

TABLE DR1: AVERAGE EROSION RATES FROM COSMOGENIC BE-10 CONCENTRATIONS

Sample	Weight (g)	Carrier (µg)	Latitude (DD)	Longitude (DD)	Avg. Elev. (m)	Stream Order	Area (km^2)	[Be-10] atoms g^{-1}	error	E (m Ma^{-1})	error
Arid Catchments											
KR-15	30.291	0.300	-23.047	31.229	324	1	0.034	572960	19352	5.90	0.65
KR-16	30.536	0.301	-23.046	31.230	345	1	0.059	598771	11727	5.70	0.60
KR-17	30.186	0.300	-23.044	31.235	346	2	0.605	531510	28449	6.55	0.78
KR-18	30.431	0.301	-23.043	31.243	323	3	10.291	620945	17978	5.36	0.59
KR-19	30.557	0.301	-23.124	31.289	403	4	757.837	687701	29690	5.07	0.59
KR-114	23.113	0.307	-23.037	31.280	400	4	---	538950	12400	6.72	0.70
Semi-Arid Catchments											
KR-1	30.848	0.301	-25.025	31.495	350	1	0.043	493396	14951	7.30	0.77
KR-2	30.248	0.301	-25.020	31.491	355	2	0.478	469055	14528	7.76	0.82
KR-4	30.123	0.299	-25.037	31.504	433	4	138.023	628558	15957	5.88	0.63
KR-5	30.418	0.300	-25.030	31.502	352	3	1.711	614836	13801	5.66	0.61
Sub-Humid Catchments											
KR-6	30.237	0.301	-25.212	31.282	563	1	0.281	975502	16819	3.90	0.44
KR-7	30.405	0.303	-25.222	31.272	586	3	35.127	1063104	17543	3.59	0.41
KR-8	30.065	0.302	-25.220	31.273	555	2	8.573	1110870	20532	3.31	0.39
KR-11	30.093	0.299	-25.236	31.267	573	4	58.755	780108	16034	5.11	0.56

Concentration errors include 1 σ from AMS. All errors propagated to average erosion rates.

Latitude and altitude production rate scaling factor used pixel-pixel for catchment-averaged rates (Dunai, 2000).

Densities: Sediment, 2.6 g cm^{-3}, for *Avg. E*; lambda 145 g cm^{-2}.

^{10}Be from rescaled sea level production rate of and 5.1 atoms g^{-1} yr^{-1} (Balco et al., 2008).

^{10}Be ratios calibrated to 07KNSTD, measured at PRIME lab AMS

Stream order based on Strahler (1957) classification.

Area-slope transition as a proxy for ridge-valley spacing and landscape dissection

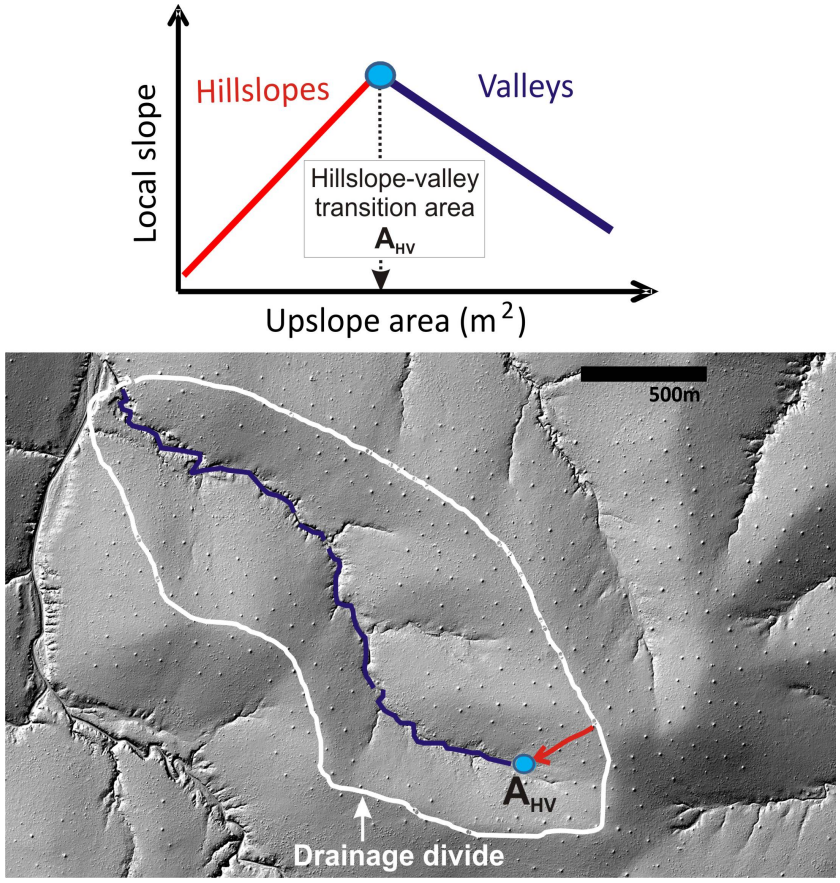

Figure DR2. Schematic of area-slope plot and corresponding location of hillslope, transition area, and valley network on a shaded relief image from our intermediate rainfall site. Slope increases downslope on hillslopes (red line) before reaching a maximum near the area of the hillslope-valley ($\mathbf{A_{HV}}$), which is shown by a light blue filled circle. At larger drainage areas, local slope decreases reflecting the tendency for channel profiles to be concave (i.e., become gentler downstream). Note that the hillslope-valley transition area is an average value and will vary within a given setting due to natural variations as well as uncertainty in the flow routing algorithm used. Importantly, our area-slope analysis averages all possible flowpaths within a 1.5km x 1.5km area (shown in Figure DR4) for each climate zone to arrive at the characteristic values of $\mathbf{A_{HV}}$, which is a proxy for ridge-valley spacing and landscape dissection. Higher values of $\mathbf{A_{HV}}$ correspond to larger ridge-valley spacing and lower valley density.

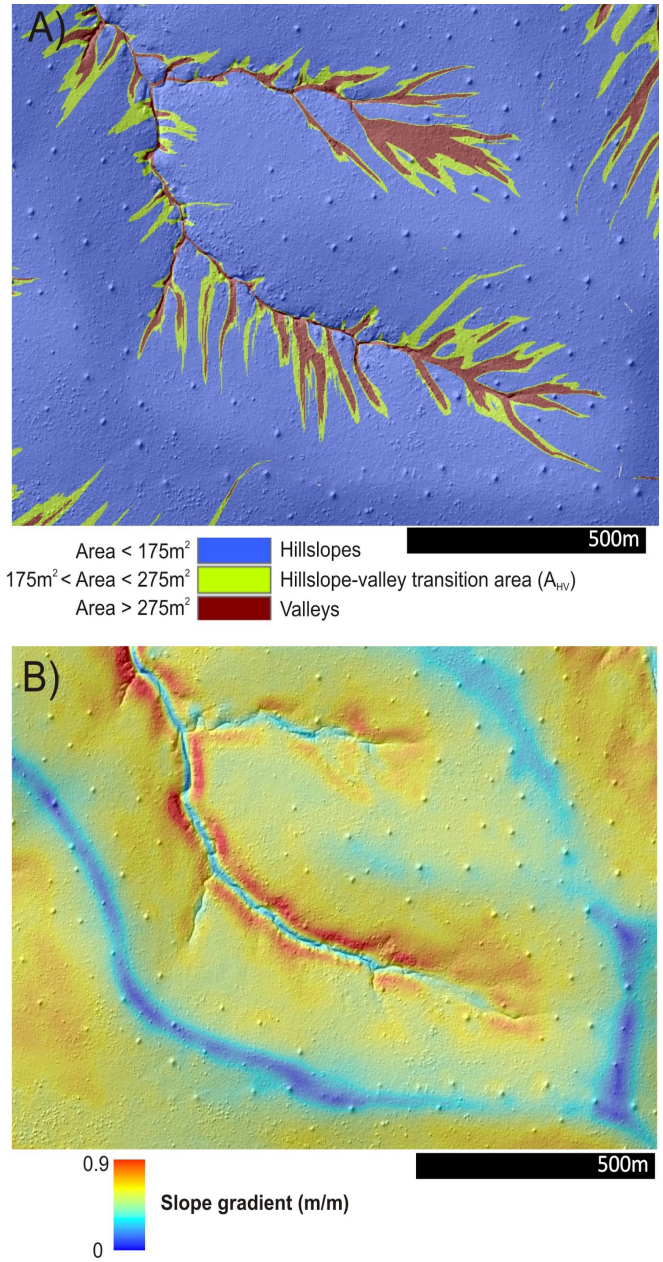

Figure DR3. Example maps of drainage area (A) and local slope (B) for a small catchment in our intermediate rainfall study site. **A)** Note that hillslopes have low drainage area (blue) and comprise the vast majority of the landscape. The transition between hillslopes and valleys at drainage areas between 175 and 275 m^2 is demarcated in yellowish-green. We averaged the areal extent of this transition for each climatic zone in our study area. Variability in the hillslope-valley transition area (A_{HV}) is apparent in A, but is not significant relative to the differences in A_{HV} that we observe amongst our study sites. Where the transition area (i.e., yellow areas) transgresses onto hillslopes, we often observe subtle, unchanneled depressions that may reflect transient adjustment to valley network dynamics. In other words, the tips of the valley network appear to be dynamic. **B)** Slope gradient for the same catchment

shown in B. Note that hilltops are gentle and hillslopes increase in steepness in the downslope direction (which defines a convex form) and tend to be steepest near the hillslope-valley transition. Because our wavelet filter effectively removes termite mounds before we smooth the topography, these 2m-high features do not influence local slope or flowpaths.

Figure DR4. Shaded relief images used for slope-area analysis (red boxes are 1.5km x 1.5km). Within each box, all data was averaged to generate relationships illustrated in Fig. 3 in the text.

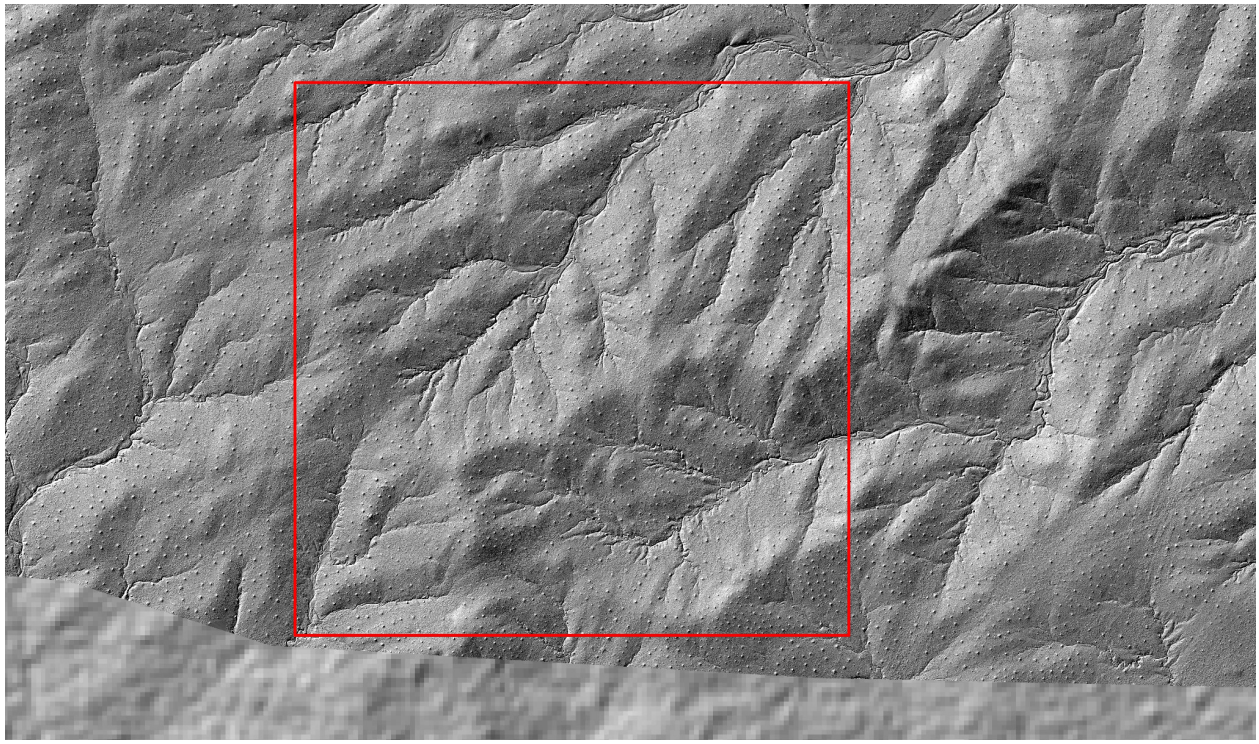

A) Phugwane area (Mean Annual Precipitation = 470 mm, lat/long: -22.999, 31.187)

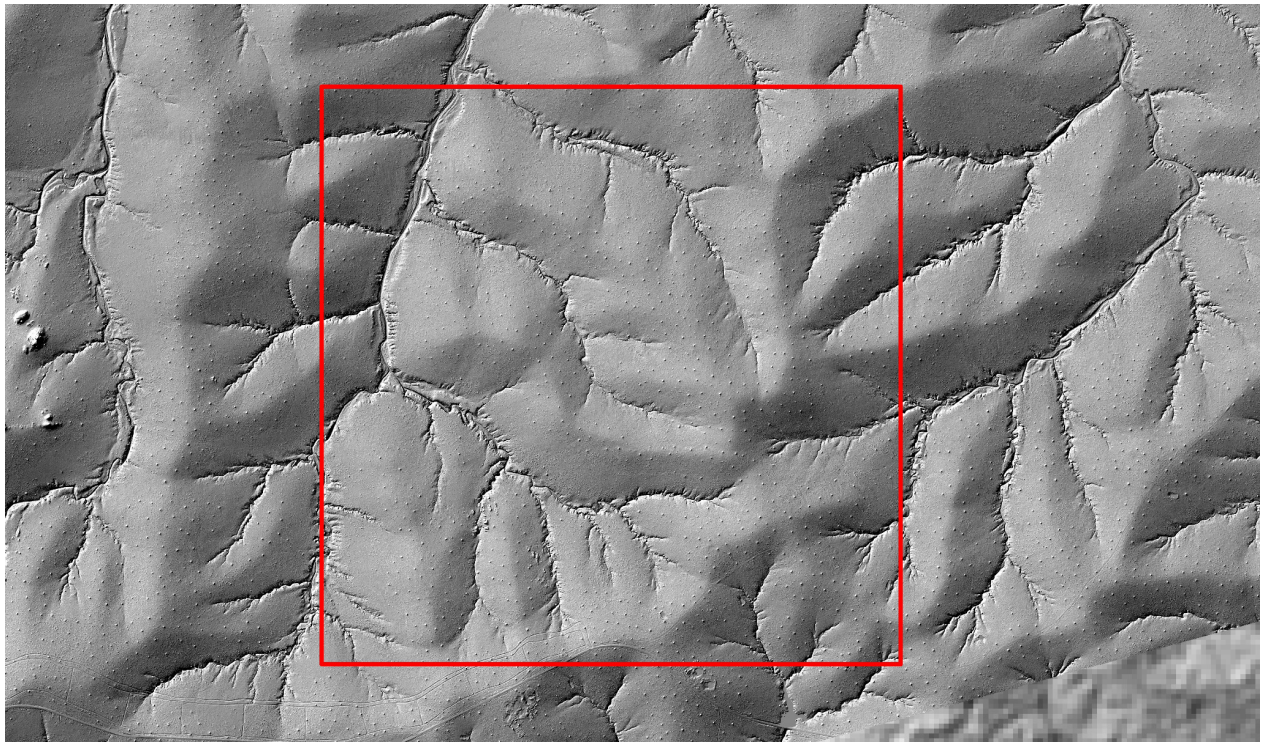

B) Skukuza area (Mean Annual Precipitation = 550 mm, lat/long: -25.082, 31.472)

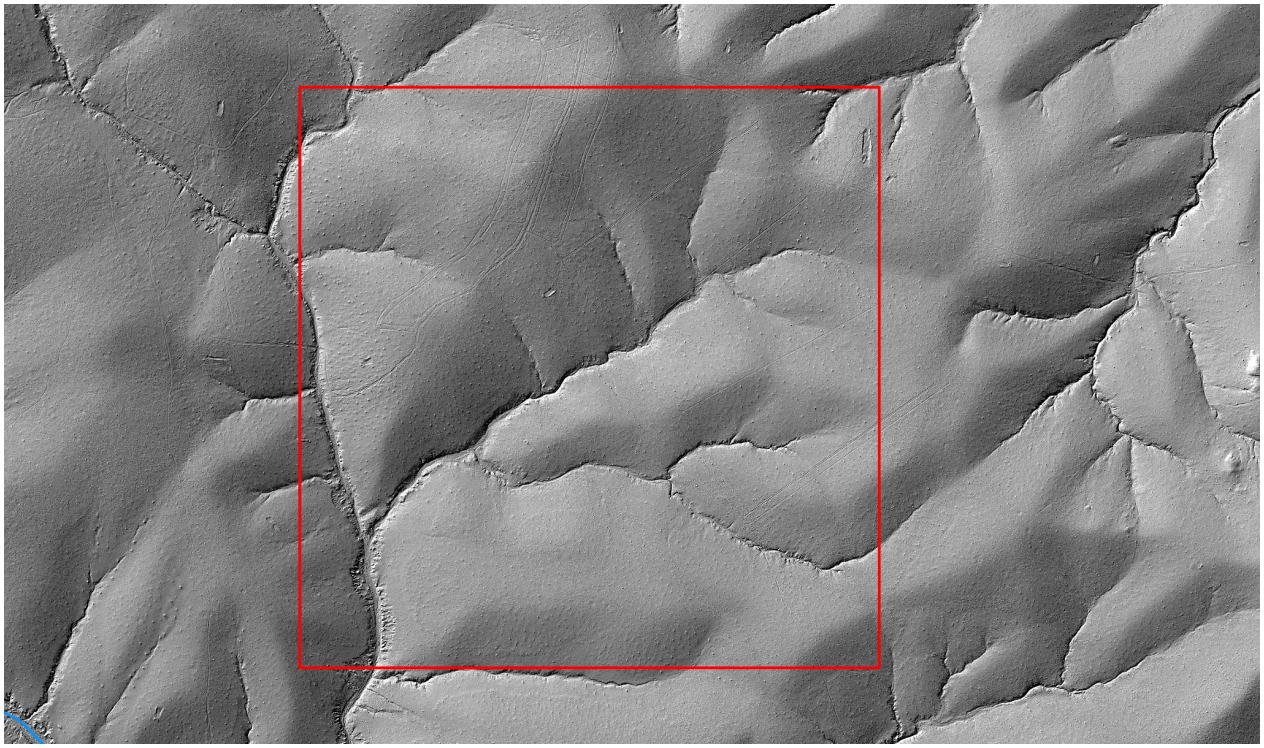

C) Pretoriuskop area (Mean Annual Precipitation = 730 mm, lat/long: -25.213, 31.287)

Quantification of Bare Ground

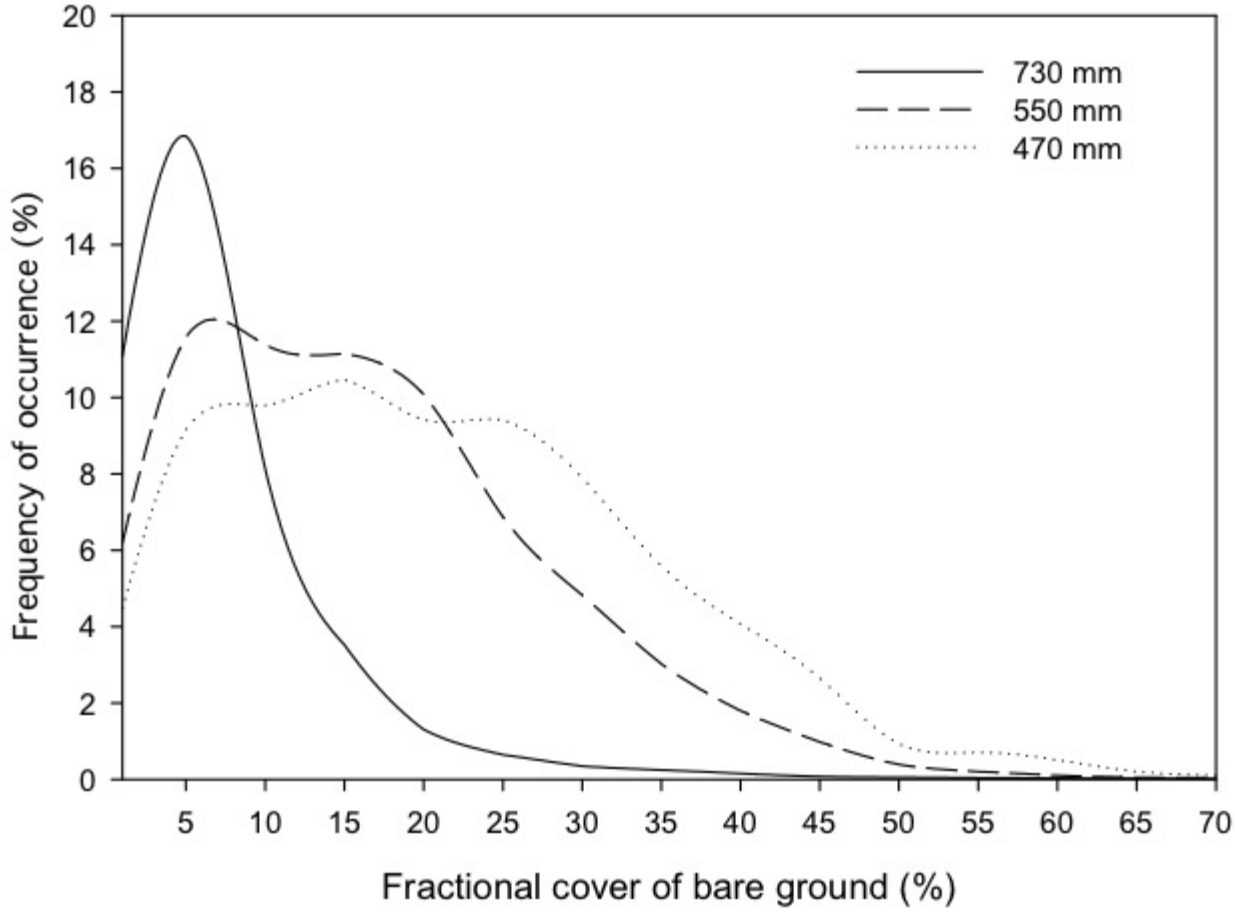

Figure DR5. Frequency distribution of bare ground for a 4.8 ha area in each rainfall zone. The area was imaged using the CAO hyperspectral instrument producing 5 m pixels. Bare ground data were separated from photosynthetic vegetation and non-photosynthetic vegetation using a pixel unmixing algorithms. Mean values for bare ground are 16.2, 9.8 and 3.7%, respectively for the 470, 550 and 730 mm rainfall sites. Data and methods are presented in Asner et al. (2009).

Hotspots of Erosion Near the Lower End of Catenas

Figure DR6. Example of soil slip near the lower edge of the clay-rich zone in the wet site near area shown in Supplementary Fig. 1, I. The channel that evacuates the local catena sediments from the catchment is located in the lower right part of the picture. The upper edge of the soil slip is about 100 m from the channel. Erosion features like this are not found higher in the landscape except where roads have artificially concentrated flow. Oblique photo taken from helicopter by Shaun Levick.

References Cited for Supplementary Materials

Asner, G. P., Levick, S. R., Kennedy-Bowdoin, T., Knapp, D.E., Emerson, R. Jacobson, J., Colgan, M. S., and Martin, R. E., 2009, Large-scale impacts of herbivores on the structural diversity of African savannas: Proceedings of the National Academy of Sciences, v. 106, p. 4947-4952.

Bern, C.R., Chadwick, O.A., Hartshorn, A.S., Khomo, L.M., and Chorover, J., 2011, A mass balance model to separate and quantify colloidal and solute redistributions: Chemical Geology v.282, p. 113–119.

Bierman, P., & Steig, E.J., 1996, Estimating rates of denudation using cosmogenic isotope abundances in sediment: Earth Surf. Processes and Landforms v. 21, P. 125–139.

Brimhall, G.H, Chadwick, O.A., Lewis, C.J., Compston, W., Dietrich, W.E., Powers, M., Hendricks, D.M., and Bratt, J., 1992, Deformational mass transport and invasive processes in soil evolution: Science, v. 255, p. 695-702.

Brown, E.T., Stallard, R.F., Larsen, M.C., Raisbeck, G.M., and Yiou, F., 1995, Denudation rates determined from the accumulation of in situ-produced 10Be in the Luquillo Experimental Forest, Puerto Rico: Earth Planet. Sci. Lett. v.129, p. 193–202.

Chase, B. M., & Meadows, M. E., 2007, Late Quaternary dynamics of southern Africa's winter rainfall zone: Earth-Science Reviews, v. 84, p. 103-138.

Dunai, T.J., 2000, Scaling factors for production rates of in situ produced cosmogenic nuclides: a critical reevaluation: Earth Planet. Sci. Lett. v.176, p. 157–169.

Gasse, F., Chalie, F., Vinces, A., Williams, M.A.J., and Williamson, D., 2008, Climatic patterns in equatorial and southern Africa from 30,000 to 10,000 years ago reconstructed from terrestrial and near-shore proxy data: Quaternary Science Reviews, v. 27, p. 2316-2340.

Granger, D.E., Kirchner, J.W., and Finkel, R.C., 1996, Spatially averaged long-term erosion rates measured from in situ-produced cosmogenic nuclides in alluvial sediment: J. Geol. v.104, p. 249–257.

Khomo, L. Bern, C.R., Hartshorn, A.S., Rogers, K.H., and Chadwick, O.A., 2013, Chemical tranfers along slowly eroding catenas developed on granitic crations in southern Africa: Geoderma, v. 202-203, p. 192-202.

Khomo, L. Hartshorn, A.S., Rogers, K.H., and Chadwick, O.A., 2011, Impact of rainfall and topography on the distribution of clays and major cations in granitic catenas in southern Africa: Catena v.87 p. 119-128.

Kohl, C.P., & Nishiizumi, K., 1992, Chemical isolation of quartz for measurement of *in-situ* produced cosmogenic nuclides: Geochim. Cosmochim. Acta v.56, p. 3583–3587.

Levick, S. R., Asner, G. P., Chadwick, O. A., Khomo, L. M., Rogers, K. H., Hartshorn, A. S., and Knapp, D. E., 2010, Regional insight into savanna hydrogeomorphology from termite mounds: Nature Communications, v.1(65), p. 1-7.

Partridge, T. C., Kerr, S. J., Metcalfe, S. E., Scott, L., Talma, A. S., & Vogel, J. C., 1993, The Pretoria saltpan: a 200,000 year southern African lacustrine sequence: Palaeogeography, palaeoclimatology, palaeoecology, v.101, p. 317-337.

Riebe, C.S., & Granger, D.E., 2013, Quantifying effects of deep and near-surface chemical erosion cosmogenic nuclides in soils, saprolite, and sediment: Earth Surface Processes and Landforms, v.38, p. 523-533.

Strahler, A.N., 1957, Quantitative analysis of watershed geomorphology: American Geophysical Union Transactions v.38, p. 913–920.

von Blanckenburg, F., 2005, The control mechanisms of erosion and weathering at basin scale from cosmogenic nuclides in river sediment: Earth Planet. Sci. Lett. v.237, p. 462–479.